Precise Control of Thermal and Redox Properties of Organic Hole-Transport Materials

Valerie A. Chiykowski[+], Yang Cao[+], Hairen Tan, Daniel P. Tabor, Edward H. Sargent,* Alán Aspuru-Guzik,* and Curtis P. Berlinguette*

Abstract: *We report design principles of the thermal and redox properties of synthetically accessible spiro-based hole transport materials (HTMs) and show the relevance of these findings to high-performance perovskite solar cells (PSCs). The chemical modification of an asymmetric spiro[fluorene-9,9′-xanthene] core is amenable to selective placement of redox active triphenylamine (TPA) units. We therefore leveraged computational techniques to investigate five HTMs bearing TPA groups judiciously positioned about this asymmetric spiro core. It was determined that TPA groups positioned about the conjugated fluorene moiety increase the free energy change for hole-extraction from the perovskite layer, while TPAs about the xanthene unit govern the T_g values. The synergistic effects of these characteristics resulted in an HTM characterized by both a low reduction potential (≈ 0.7 V vs. NHE) and a high T_g value ($> 125°C$) to yield a device power conversion efficiency (PCE) of 20.8% in a PSC.*

Hole-transport materials (HTMs) are a key component of organic light-emitting diodes (OLEDs)[1–3] and solid-state solar cell devices.[4,5] High performance HTMs for perovskite solar cells (PSCs) should exhibit high glass transition temperatures (T_g) to suppress the formation of grain boundaries in glassy films which can impede effective charge transfer.[6,7] A favourable band alignment between the perovskite valence band to HTM (HOMO) level is necessary to promote efficient charge extraction from the photoexcited perovskite layer to the contacts.[8,9] These materials should also have high temporal stability under elevated temperatures and humidity.[10–12]

Organic HTMs are amenable to low-temperature solution processing while also being capable of mediating high power conversion efficiencies (PCEs).[13,14] Spiro-OMeTAD[15] (Figure 1) is a widely used organic HTM and is capable of
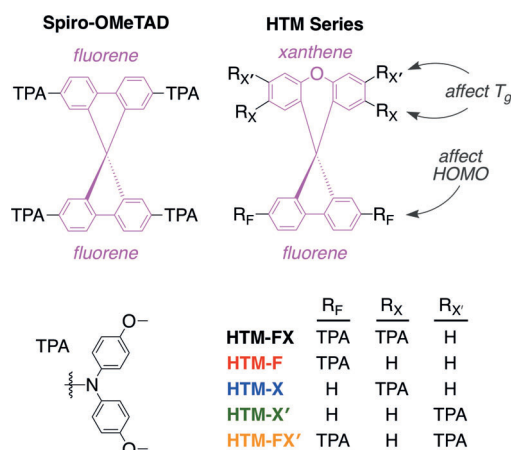

Figure 1. Molecular representations of Spiro-OMeTAD[15] and the HTM series under investigation.

reaching PCEs greater than 20% when integrated in PSCs.[16,17] However, Spiro-OMeTAD is expensive to manufacture because the tetrahedral spiro carbon that bridges the two perpendicular fluorene moieties (9,9′-spirobifluorene) can only be accessed through a succession of substitution, lithiation, condensation and bromination steps.[18] Notwithstanding, the molecule teaches how a spiro carbon center can impart a rigid 3D structure that leads to a high T_g (125°C).[19] The redox-active TPA substituents functionalized with methoxy groups also yield reversible redox couples at potentials appropriate for use in a PSC.[20] This combination of structural and electrochemical properties contributes to the high hole mobilities (2×10^{-4} to 5×10^{-5} cm^{2}V^{-1}s^{-1}) that have proven so effective for Spiro-OMeTAD.[21]

[*] V. A. Chiykowski,[+] Dr. Y. Cao,[+] Prof. Dr. C. P. Berlinguette
    Department of Chemistry, The University of British Columbia
    2036 Main Mall, Vancouver, British Columbia, V6T 1Z1 (Canada)
    E-mail: cberling@chem.ubc.ca

    Dr. H. Tan, Prof. Dr. E. H. Sargent
    Department of Electrical and Computer Engineering
    University of Toronto
    10 King's College Road, Toronto, Ontario, M5S 3G4 (Canada)
    E-mail: ted.sargent@utoronto.ca

    Dr. D. P. Tabor, Prof. Dr. A. Aspuru-Guzik
    Department of Chemistry and Chemical Biology, Harvard University
    12 Oxford St., Cambridge, MA 02138 (USA)
    E-mail: alan@aspuru.com

    Prof. Dr. A. Aspuru-Guzik
    Department of Chemistry and Department of Computer Science,
    University of Toronto, Toronto, Ontario M5S 3H6 (Canada)
    and
    Vector Institute, Toronto, ON M5G 1M1 (Canada)

    Prof. Dr. C. P. Berlinguette
    Department of Chemical and Biological Engineering
    The University of British Columbia
    2360 East Mall, Vancouver, British Columbia, V6Y 1Z3 (Canada)
    and
    Stewart Blusson Quantum Matter Institute
    The University of British Columbia
    2355 East Mall, Vancouver, British Columbia, V6T 1Z4 (Canada)

[+] These authors contributed equally to this work.

  Supporting information and the ORCID identification number(s) for the author(s) of this article can be found under https://doi.org/10.1002/anie.201810809.

Hagfeldt and Sun,[22] and Robertson[23] and their respective co-workers recently independently disclosed that the alternative spiro-based HTM "X60" exhibits performance parameters competitive to Spiro-OMeTAD. X60, denoted herein as **HTM-FX** (Figure 1), is an important discovery because the core can be synthesized using a one-pot condensation reaction between phenols and a fluorenone moiety. This condensation yields juxtaposed fluorene and xanthene units at a tetrahedral carbon centre. This asymmetric fluorene-9,9′-xanthene core can be functionalized with TPA groups, analogous to that of Spiro-OMeTAD, to generate hole-transport properties that produce high PCEs in PSCs.[20,22,23]

The simple reaction chemistry associated with spiro-based **HTM-FX** inspired us to elucidate how each of the TPA units about the asymmetric spiro core affects the HTM properties and the corresponding performance in a PSC. We discovered that the TPA groups positioned about the highly conjugated fluorene fragment are the relevant electrochemically active units (i.e., associated with the redox couple that represents the HOMO energy level, E_{HOMO}) while those positioned on the xanthene moiety affect the structural and thermal properties. We were able to resolve this structure-property relationship by placing TPA groups exclusively on the fluorene (**HTM-F**) or the xanthene (**HTM-X**) units. These results pointed to the xanthene substituents governing the thermal properties, prompting us to test how *para-* and *meta-* substitution of TPAs at the xanthene moiety (i.e., **HTM-X** and **HTM-X′**) affects the thermal properties. This decoupling of the E_{HOMO} levels and bulk thermal properties (e.g., T_g) yielded **HTM-FX′** characterized by a distinctively higher T_g of 137 °C. This HTM was found to be capable of generating a PCE of 20.8 % in a PSC, a value that compares favorably with those measured for Spiro-OMeTAD and **HTM-FX** under the same experimental conditions. Moreover, devices containing **HTM-FX′** could be prepared with a notably high level of reproducibility. This identification of how the TPAs impact the redox activity, thermal properties and device characteristics will guide the design of new high-performance asymmetric HTMs.

Replacing one of the two fluorene units in Spiro-OMeTAD with a xanthene unit to form **HTM-FX**[22,23] enables us to test which specific TPA groups affect the redox properties and thermal temperatures of HTMs. We used computational methods to screen the five HTMs in Figure 1 containing this asymmetric core for appropriate frontier orbital energy levels, low reorganization energies and photophysical properties. The frontier orbitals were modeled (Figure S1) and the DFT-computed reduction potentials corresponding to the first oxidation event (ε_{HOMO}, Table S1) were predicted to all exhibit suitable reduction potentials for hole extraction from the perovskite layer. The reorganization energies (E_{reorg}) for the entire **HTM** series (Table S1) were evaluated using Nelsen's four point method.[22,24,25] HTMs containing TPA moieties at the R_x or $R_{x'}$ positions of the HTM scaffold were predicted to exhibit smaller E_{reorg} values that are favorable for efficient hole transport according to Marcus theory.[26] The vertical electron affinity of the cation at the adiabatic cation minimum appears to be the more

dominant factor that affects E_{reorg}, and **HTM-F** was found to contain the largest relative contribution from this term. Modeling the spin-density differences of the adiabatic minima for the singly oxidized molecules of the series (Figure S2) provides a visualization of the hole on an oxidized HTM and reveals differences in hole delocalization within the series. Fluorene was confirmed to be a highly conjugated unit and the positions of TPA groups on the xanthene moieties affect the electronic structure of the oxygen bridge. All computed E_{reorg} (0.14–0.20 eV) were close to that of Spiro-OMeTAD (0.14 eV).

The preparation of **HTM-FX** followed a modified literature procedure where 2,7-dibromofluorenone was reacted with 4-bromophenol to yield a tetra-brominated product that, in turn, undergoes a Pd-catalyzed Buchwald-Hartwig coupling with 4,4′-dimethoxyphenylamine to yield the product.[22] This procedure was adapted to access the rest of the **HTM** series (Scheme S1) using either non-brominated fluorenone for **HTM-X** and **HTM-X′** and/or 3-bromophenol for **HTM-FX′** and **HTM-X′**. All compounds in the **HTM** series were prepared in merely two reaction steps under relatively benign reaction conditions and a single column purification step. By contrast, the Spiro-OMeTAD core requires a multi-step synthesis involving highly air and moisture-sensitive reagents, hazardous lithiation reactions and several time-consuming column chromatographic purification steps.[15]

The melting point (T_m) and T_g of each HTM measured by differential scanning calorimetry (DSC) is tabulated in Table 1. The T_m and T_g values for every member of the

Table 1: Electrochemical and hole-transport properties of HTMs.

Compound	E_{HOMO}[a] (V vs. NHE)	ε_{HOMO}[b] (eV)	T_g[c] [°C]	Hole mobility[d] [×10^{-4} cm^2 V^{-1} s^{-1}]
Spiro-OMeTAD	0.63	−5.13	125	6.9
HTM-FX	0.67	−5.17	107	1.4
HTM-F	0.67	−5.17	104	0.4
HTM-X	0.76	−5.26	94	0.5
HTM-X′	0.97	−5.47	130	0.3
HTM-FX′	0.66	−5.16	137	4.8

[a] The half-wave potential corresponding to the first oxidation process in the cyclic voltammogram. Measured in DCM and referenced to NHE by addition of ferrocene. [b] $\varepsilon_{HOMO} = -(eE_{HOMO} + 4.50 \text{ eV})$. [c] Determined by DSC. All T_m values determined to be > 300 °C and above the detection limits of our instrument. [d] Determined by space-charge-limit current (SCLC) method from doped HTMs.

series were measured to be > 300 °C and > 93 °C, respectively. A minimum T_g value of 90 °C is required to avoid morphology changes during solar cell operation.[6] There is no apparent trend between number of TPA units and glass transition temperature. However, substitution at the *meta-*position of the xanthene moiety was found to increase T_g by over 30 °C (e.g., T_g (**HTM-X′**) = 130 °C c.f. T_g (**HTM-X**) = 94 °C). This marked increase in T_g through *meta-*substitution of the xanthene was also observed in the case of **HTM-FX′** (T_g = 137 °C c.f. T_g(**HTM-FX**) = 107 °C).

Cyclic voltammograms (CVs) for each HTM was recorded in 0.1 M n-NBu$_4$PF$_6$ DCM solutions to determine the E_{HOMO} for the series (Table 1 and Figure S15). The E_{HOMO}

values for HTMs bearing TPAs on the fluorene (**HTM-F**, **HTM-FX**, and **HTM-FX'**) were all found to be ≈ 0.66 V vs. NHE, which is slightly more positive than Spiro-OMeTAD (0.63 V vs. NHE) and therefore appropriate for energy alignment with the perovskite layer. Differential pulse voltammetry (DPV) was used to deconvolute and quantify each of the successive oxidation events for the series (Figure 2
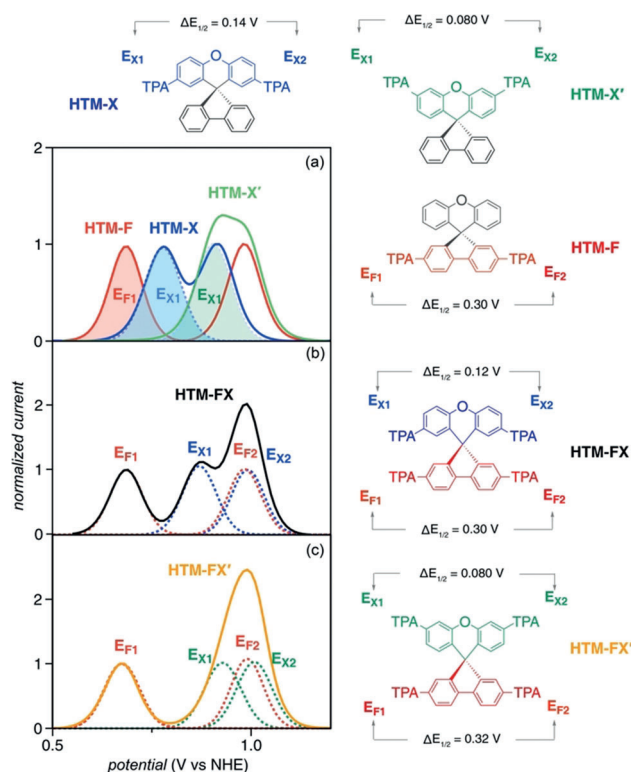

Figure 2. Differential pulse voltammograms (DPVs) for HTM series normalized to their first oxidation event. The number of electrons that contribute to each redox process was determined by integrating the area beneath the peak fitting. a) The first deconvoluted oxidation events are shown in shaded colors to highlight the progressively anodic shift of E_{HOMO} for **HTM-F**, **HTM-X** and **HTM-X'**, respectively. Traces for b) **HTM-FX** and c) **HTM-FX'** are deconvoluted to highlight that the E_{HOMO} is linked to the TPA unit positioned on the fluorene unit.

and Table S3). The number of oxidation events tracked the number of TPA units on the HTM, and we were able to assign the redox activity to each TPA unit by taking a number of different observations into account. For example, the E_{HOMO} levels for the HTMs with only *para*- or *meta*-substituted xanthene TPAs (**HTM-X** and **HTM-X'**, respectively) are higher than that of the HTM with only fluorene TPAs (**HTM-F**) and reflect a lower degree of electronic coupling based on successive oxidation of their two TPA groups (Figure 2 a). This conjecture is fully supported by the trend in DFT computed ε_{HOMO} values (Table S1). The first reduction potentials (E_{HOMO}) for **HTM-FX** and **HTM-FX'** can therefore be linked to the first oxidations of the fluorene TPAs (E_{F1}), in that the first oxidation event of **HTM-FX** and **HTM-FX'** matches that measured for **HTM-F** (0.67 V vs. NHE). The second oxidation event for **HTM-FX** at 0.87 V vs. NHE is

attributed to the first oxidation of the xanthene TPAs (E_{X1}) by benchmarking against **HTM-X** (0.78 V vs. NHE). We can assign the third and fourth oxidations events of **HTM-FX** to the second faradaic events for **HTM-F** (E_{F2}) and **HTM-X** (E_{X2}) according to their electronic coupling ($\Delta E_{1/2}$ in Figure 2) with the first two oxidations. Similarly, all four oxidation events for **HTM-FX'** have been resolved even though the second to fourth oxidation features overlapped significantly and appeared to be a three-electron process (0.8 to 1.1 V vs. NHE). Modeling the degree of hole delocalization of the cationic HTM species (Figure S2) provides a visualization of the hole on an oxidized HTM and clearly shows that the relevant redox activity is confined to the TPA groups appended to the fluorene units. This finding indicates that the xanthene units can be modified without compromising the E_{HOMO} levels corresponding to the fluorene TPA units. The similar UV-visible absorption and emission maxima (Table S2) of **HTM-F**, **HTM-FX** and **HTM-FX'** confirm the similar electronic structures of the compounds' frontier orbitals. All HTMs under study have limited light absorption in the visible region which may be beneficial in maximizing light absorption by the perovskite layer (Figure S14).

The hole mobilities were determined using the space-charge-limited current (SCLC) method (Table 1). The *J–V* characteristics of hole-only devices with various HTMs are shown in Figure 3 a. The HTMs were doped with 4-*tert*-butylpyridine (*t*BP) and bis(trifluoromethane)sulfonimide lithium salt (LiTFSI). The mobilities of Spiro-OMeTAD, **HTM-FX** and **HTM-FX'** obtained here are comparable to previously reported values.[21,22,27] The mobility of **HTM-FX'** is close to that of Spiro-OMeTAD and is much higher than that of all other HTM compounds in the series under study. While the E_{HOMO} level of **HTM-FX'** is similar to **HTM-FX**, the higher mobility is ascribed to the *meta*-substitution
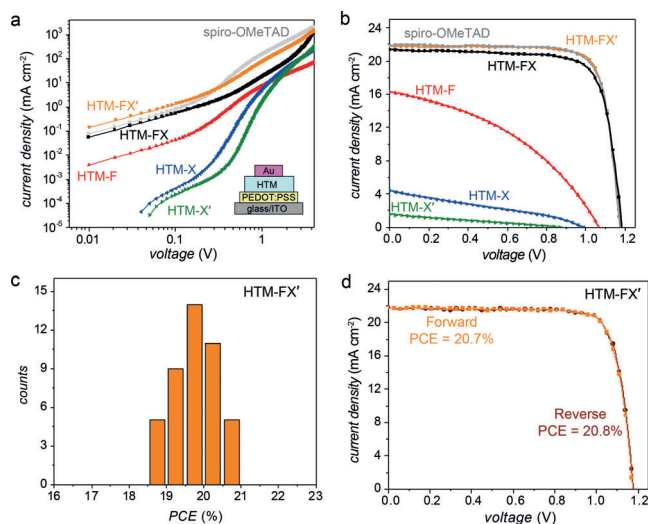

Figure 3. Performance of perovskite solar cells with HTMs: a) *J–V* curves of hole-only devices with various HTMs; b) *J–V* curves of solar cells with various HTMs measured under solar simulator (100 mWcm⁻²); c) Histogram of PCEs for 44 devices with **HTM-FX'**; d) *J–V* curves of champion device with **HTM-FX'** scanned in reverse and forward directions (scanning rate of 20 mVs⁻¹).

affecting the chemical structure or electronic delocalization. The low hole mobilities of **HTM-X** and **HTM-X′** may be due to the E_{HOMO} levels being too high in energy for efficient doping by LiTFSI. Given that the extent of hole doping for **HTM-F** and **HTM-FX** by LiTFSI is expected to be similar based on the similarities in E_{HOMO}, the low mobility of **HTM-F** is attributed to the higher E_{reorg} value (0.21 eV) relative to the other HTMs (< 0.16 eV). Each of the HTMs were then tested in planar PSCs with the device architecture glass/ITO/TiO₂-Cl/perovskite/HTM/Au.[17] Table 2 summarizes the statistical

Table 2: Statistical performance data of HTM series in perovskite devices.[a]

Compound	V_{oc} [V]	J_{sc} [mA cm^{-2}]	FF	PCE [%]	Champion PCE [%]
Spiro-OMeTAD	1.16(2)	21.9(3)	0.78(2)	19.7(5)	20.4
HTM-FX	1.16(1)	21.2(3)	0.74(2)	18.2(7)	19.5
HTM-F	1.08(2)	14.7(9)	0.41(2)	6.5(5)	7.0
HTM-X	0.88(11)	3.8(6)	0.32(2)	1.1(2)	1.3
HTM-X′	0.77(6)	1.4(1)	0.26(1)	0.2(1)	0.3
HTM-FX′	1.17(1)	21.7(3)	0.78(2)	19.7(6)	20.8

[a] Statistical performance of 41 Spiro-OMeTAD devices, 24 **HTM-FX** devices, 44 **HTM-FX′** devices, 8 **HTM-F** devices, and 4 devices for each **HTM-X** and **HTM-X′**, is shown here.

performance of devices fabricated with otherwise-identical device processing for each HTM, and the *J–V* curves of champion devices for each HTM are shown in Figure 3b.

The HTMs exhibit similar charge extraction kinetics and effective photoluminescence quenching for all HTMs as revealed by time-resolved and steady-state photoluminescence (PL) measurements (Figure S17). Hole extraction from the perovskites to each of the HTMs in this study was not found to be a limiting factor, except for **HTM-X′** which showed incomplete PL quenching (Figure S17a). The HTMs exhibit similar charge extraction kinetics between Spiro-OMeTAD, **HTM-FX**, and **HTM-FX′** (Figure S17b) though the initial PL decay rates in HTMs with only two TPA moieties follow the trend of **HTM-F** > **HTM-X** > **HTM-X′** (Figure S17c).

PSCs containing **HTM-F**, **HTM-X**, and **HTM-X′** all generated low PCE values. This observation is attributed to the low hole mobilities (Table 1) precluding effective transport of carriers through the HTM layers. **HTM-FX** results in PCEs that are lower than Spiro-OMeTAD and the best device yielded a PCE of 19.5% which is comparable to a previous report.[22] **HTM-FX′** outperformed **HTM-FX** (20.8% vs. 19.5%, respectively) and the performance enhancement can be attributed to the 3-fold higher hole mobility imparted by the change of TPA substitution pattern on the xanthene group (4.8 vs. 1.4×10^{-4} cm^{2}V^{-1}s^{-1}, respectively). **HTM-FX′** produced a device performance that rivals that of Spiro-OMeTAD. PSCs containing **HTM-FX′** exhibit excellent reproducibility, as indicated by the narrow PCE distribution over 44 devices (Figure 3c). Moreover, PSCs containing **HTM-FX′** also show negligible hysteresis in the *J–V* measurements (Figure 3d and Figure S16a). These results highlight

the *meta*-substitution of the xanthene groups to be an important handle for achieving high-efficiency PSCs.

Breaking the symmetric core of Spiro-OMeTAD by replacing one of the two fluorene units with a xanthene unit to form **HTM-FX**[22] enabled us to experimentally resolve how the positions of TPA groups about the core affect the redox properties and glass transition temperatures of HTMs relevant to high efficiency PSCs. TPA groups positioned on the highly conjugated fluorene moiety renders the HTM easier to oxidize, which, in turn, increases the free energy change for hole-extraction from the perovskite layer. The glass transition temperatures, however, are governed by the TPAs about the xanthene unit. Substitution at the *meta*-position raises the T_g by 30°C over those substituted at the *para*-position. The synergistic effects of a positively shifted E_{HOMO} and high glass transition temperature in **HTM-FX′** yielded a maximum device power conversion efficiency of 20.8%, which is commensurate with current state-of-the-art PSCs. Electrochemical, photophysical and structural findings were fully supported by computational analysis of the frontier orbital and reorganization energies of the neutral HTMs and spin density difference maps of cationic species, thereby highlighting the role predictive tools can play in screening future state-of-the-art HTMs. This set of design principles that enables selective control of redox and mesoscopic properties of asymmetric HTMs will be elaborated on in future studies in pursuit of robust higher performance PSCs.

Conflict of interest

The authors declare no conflict of interest.

[1] M. Mesta, M. Carvelli, R. J. de Vries, H. van Eersel, J. J. M. van der Holst, M. Schober, M. Furno, B. Lüssem, K. Leo, P. Loebl, et al., *Nat. Mater.* **2013**, *12*, 652–658.

[2] X. Liang, K. Wang, R. Zhang, K. Li, X. Lu, K. Guo, H. Wang, Y. Miao, H. Xu, Z. Wang, *Dyes Pigm.* **2017**, *139*, 764–771.

[3] D. F. O'Brien, P. E. Burrows, S. R. Forrest, B. E. Koene, D. E. Loy, M. E. Thompson, *Adv. Mater.* **1998**, *10*, 1108–1112.

[4] L. Calió, S. Kazim, M. Grätzel, S. Ahmad, *Angew. Chem. Int. Ed.* **2016**, *55*, 14522–14545; *Angew. Chem.* **2016**, *128*, 14740–14764.

[5] Z. H. Bakr, Q. Wali, A. Fakharuddin, L. Schmidt-Mende, T. M. Brown, R. Jose, *Nano Energy* **2017**, *34*, 271–305.

[6] J. Wu, Z. Lan, J. Lin, M. Huang, Y. Huang, L. Fan, G. Luo, *Chem. Rev.* **2015**, *115*, 2136–2173.

[7] Y. Wang, T.-S. Su, H.-Y. Tsai, T.-C. Wei, Y. Chi, *Sci. Rep.* **2017**, *7*, 7859.

[8] L. E. Polander, P. Pahner, M. Schwarze, M. Saalfrank, C. Koerner, K. Leo, *APL Mater.* **2014**, *2*, 081503.

[9] A. Krishna, D. Sabba, J. Yin, A. Bruno, L. J. Antila, C. Soci, S. Mhaisalkar, A. C. Grimsdale, *J. Mater. Chem. A* **2016**, *4*, 8750–8754.

4   www.angewandte.org

© 2018 Wiley-VCH Verlag GmbH & Co. KGaA, Weinheim

Angew. Chem. Int. Ed. **2018**, *57*, 1–6

↖↖ These are not the final page numbers!

[10] J. Xu, O. Voznyy, R. Comin, X. Gong, G. Walters, M. Liu, P. Kanjanaboos, X. Lan, E. H. Sargent, *Adv. Mater.* **2016**, *28*, 2807 – 2815.

[11] C. Kou, S. Feng, H. Li, W. Li, D. Li, Q. Meng, Z. Bo, *ACS Appl. Mater. Interfaces* **2017**, *9*, 43855 – 43860.

[12] Y. Wang, S. Zhang, J. Wu, K. Liu, D. Li, Q. Meng, G. Zhu, *ACS Appl. Mater. Interfaces* **2017**, *9*, 43688 – 43695.

[13] P. Agarwala, D. Kabra, *J. Mater. Chem. A* **2017**, *5*, 1348 – 1373.

[14] K. Rakstys, M. Saliba, P. Gao, P. Gratia, E. Kamarauskas, S. Paek, V. Jankauskas, M. K. Nazeeruddin, *Angew. Chem. Int. Ed.* **2016**, *55*, 7464 – 7468; *Angew. Chem.* **2016**, *128*, 7590 – 7594.

[15] U. Bach, D. Lupo, P. Comte, J. E. Moser, F. Weissörtel, J. Salbeck, H. Spreitzer, M. Grätzel, *Nature* **1998**, *395*, 583 – 585.

[16] D. Bi, W. Tress, M. I. Dar, P. Gao, J. Luo, C. Renevier, K. Schenk, A. Abate, F. Giordano, J.-P. Correa Baena, et al., *Sci. Adv.* **2016**, *2*, e1501170.

[17] H. Tan, A. Jain, O. Voznyy, X. Lan, F. P. García de Arquer, J. Z. Fan, R. Quintero-Bermudez, M. Yuan, B. Zhang, Y. Zhao, et al., *Science* **2017**, *355*, 722 – 726.

[18] N. J. Jeon, H. G. Lee, Y. C. Kim, J. Seo, J. H. Noh, J. Lee, S. I. Seok, *J. Am. Chem. Soc.* **2014**, *136*, 7837 – 7840.

[19] R. Pudzich, T. Fuhrmann-Lieker, J. Salbeck, *Emissive Materials Nanomaterials*, Springer Berlin Heidelberg, Berlin, **2006**, pp. 83 – 142.

[20] J. Zhang, B. Xu, L. Yang, C. Ruan, L. Wang, P. Liu, W. Zhang, N. Vlachopoulos, L. Kloo, G. Boschloo, et al., *Adv. Energy Mater.* **2018**, *8*, 201701209.

[21] H. J. Snaith, M. Grätzel, *Appl. Phys. Lett.* **2006**, *89*, 262114.

[22] B. Xu, D. Bi, Y. Hua, P. Liu, M. Cheng, M. Grätzel, L. Kloo, A. Hagfeldt, L. Sun, *Energy Environ. Sci.* **2016**, *9*, 873 – 877.

[23] M. Maciejczyk, A. Ivaturi, N. Robertson, *J. Mater. Chem. A* **2016**, *4*, 4855 – 4863.

[24] W.-Q. Deng, W. A. Goddard, *J. Phys. Chem. B* **2004**, *108*, 8614 – 8621.

[25] S. F. Nelsen, S. C. Blackstock, Y. Kim, *J. Am. Chem. Soc.* **1987**, *109*, 677 – 682.

[26] R. A. Marcus, *J. Chem. Phys.* **1956**, *24*, 966 – 978.

[27] K. Liu, Y. Yao, J. Wang, L. Zhu, M. Sun, B. Ren, L. Xie, Y. Luo, Q. Meng, X. Zhan, *Mater. Chem. Front.* **2016**, *1*, 100 – 110.

© 2018 Wiley-VCH Verlag GmbH & Co. KGaA, Weinheim
www.angewandte.org **5**
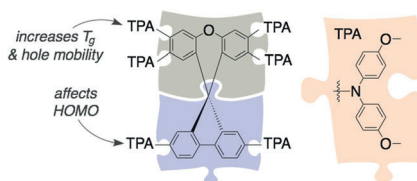
These are not the final page numbers! ↗↗

Communications

Hole-Transport Materials

V. A. Chiykowski, Y. Cao, H. Tan,
D. P. Tabor, E. H. Sargent,*
A. Aspuru-Guzik,*
C. P. Berlinguette* —————— ▮▮▮▮–▮▮▮▮

Precise Control of Thermal and Redox
Properties of Organic Hole-Transport
Materials

Design principles of the thermal and redox properties of spiro-based hole transport materials (HTMs) were developed and the relevance of these findings to high-performance perovskite solar cells (PSCs) is shown. The studies resulted in an HTM characterized by both a low reduction potential (0.7 V) and a high T_g value ($> 125\,°C$) to yield a device power conversion efficiency (PCE) of 20.8% in a PSC.